Invited feature article

Photochemical properties of a Re(I) polymer containing dppz in its structure. An interplay between dark and bright states of dppz

Alejandra Saavedra Moncada[a], Eduart Gutiérrez-Pineda[b], Iván Maisuls[a], Gustavo T. Ruiz[a], Alexander G. Lappin[c,*], Guillermo J. Ferraudi[d], Ezequiel Wolcan[a,*]

[a] Instituto de Investigaciones Fisicoquímicas Teo'ricas y Aplicadas (INIFTA, UNLP, CCT La Plata-CONICET), Diag. 113 y 64, Sucursal 4, C.C. 16, (B1906ZAA) La Plata, Argentina
[b] Universidad Nacional De La Plata, Facultad de Ingeniería, Argentina
[c] Department of Chemistry and Biochemistry, Univ. of Notre Dame, Notre Dame, IN 46556, United States
[d] Radiation Research Building, Univ. of Notre Dame, Notre Dame, IN 46556, United States

ABSTRACT

A new polymer, **P4VP-Re(dppz),** based on the poly-4-vinylpyridine structure containing $Re(CO)_3(dppz)^+$ pendants was synthesized. Multiple morphologies of **P4VP-Re(dppz),** such as vesicles, spherical nanoaggregates, large vesicle compounds, rings and pyramidal structures were observed by AFM and TEM in cast films of **P4VP-Re(dppz)** in solvents of different polarity and solvent/acid mixtures. Several conformations of a model monomer of **P4VP-Re(dppz)** were studied by TD-DFT to ascertain the effect of protonation over the molecular structure as well as over the absorption spectroscopy of **P4VP-Re(dppz)**. **P4VP-Re(dppz)** excited states and their redox reactivity towards the sacrificial reductant TEOA were studied by flash photolysis experiments either in DMF and in $DMF/HClO_4$. Those experiments were compared to the ones derived from thermal reactions of **P4VP-Re(dppz)** with solvated electrons in pulse radiolysis experiments. All the photophysical and photochemical properties studied were rationalized in terms of an interplay between $^3IL(\pi\pi^*)$, $^3MLCT(phz)$ and the $^3MLCT(phen)$ states.

© 2017 Elsevier B.V. All rights reserved.

1. Introduction

Early studies on dipyridil[3,2-a:2′3′-c]phenazine (dppz) complexes coordinated to Ru(II), such as in $[Ru(bpy)_2(dppz)]^{2+}$, outlined some very interesting features of those systems, namely that[1]: (i) $[Ru(L)_2(dppz)]^{2+}$ emitted in organic solvents but not in aqueous media, with a preferential charge transfer to dppz in the excited state, (ii) by intercalating $[Ru(bpy)_2(dppz)]^{2+}$ into DNA structure the emission could be recovered. This latter fact opened the possibility to use these complexes in the so called "light switch" effect: emission could be turned on/off by placing those complexes in an organic/aqueous media environment. Later on, fac-[Re(CO)_3(L)dppz] complexes were synthesized and intercalated to DNA showing that the "light switch" effect occurred also with these Re-tricarbonyl dppz complexes [2–6]. One triplet intra-ligand state, $^3IL(\pi\pi^*)$, and two low-lying metal to ligand charge transfer (^3MLCT) states have been suggested for explaining many

photophysical and theoretical studies on Re(I)-and Ru(II)-dppz complexes. The MLCT states have been distinguished as one MLCT (phz), i.e. an MLCT where the phenazine-like molecular orbital (MO) is populated and one MLCT(phen), where the electronic charge is transferred to the phenanthroline-like MO. The luminescence behavior of those complexes was rationalized in terms of an interplay between the $^3MLCT(phz)$ and the ^3MLCT(phen) states, the former being a non-emissive (dark) state while the latter being a luminescent (bright) state [7]. Additionally, the participation of other MLCT excited states, different from MLCT (phz) or MLCT(phen) and whose energy is modulated by the medium, has been described in fac-[(4,4′-bpy)Re(CO)_3(dppz)]^+ [8]. Several systematic absorption, emission, EPR and TRIR studies as well as DFT calculations on fac-[Re(CO)_3(X_2-dppz)py]^+ (X = H, F or CH_3) and fac-[Re(CO)_3(X_2-dppz)Cl] (X = CH_3, H, F, Cl or CF_3) have shed light on the solvent-dependent photophysical properties of those Re(I)-tricarbonyl dppz complexes. For fac-[Re(CO)_3(X_2-dppz) py]^+ in MeCN, the $^3IL(\pi\pi^*)$ dominates the photophysical properties. In aqueous solutions, the main species for the X = H and CH_3 complexes is also the $^3IL(\pi\pi^*)$ [1]. On the other hand, for the non-emissive (X = F) complex, a mix of $^3IL(\pi\pi^*)$ and MLCT(phz) occurs. A deactivation mechanism involving the formation of (H_2O) H-

---

* Corresponding authors.
  E-mail addresses: alexander.g.lappin.1@nd.edu (A.G. Lappin), gferraud@nd.edu (G.J. Ferraudi), wolcan@inifta.unlp.edu.ar (E. Wolcan).

bonding to the aza N atoms of dppz has been proposed, thus shortening the lifetime of MLCT(phz), keeping an analogy to the behavior of Ru(II)-dppz complexes [1]. Calculations on *fac*-[Re (CO)$_3$(X$_2$-dppz)Cl] show a dppz-based LUMO which is localized on the phenazine part of the dppz. More polar solvents, depending on their H-bonding ability, stabilize more the ^{3}MLCT(phz) than the ^{3}MLCT(phen) state. As a result, in Re(I) complexes, the higher lying ^{3}MLCT(phen) is preferentially populated over the lower energy MLCT(phz) [1]. By varying the electron-withdrawing ability of X on the derivatized dppz ligand the nature of the excited state could be tuned. When X = CF$_3$, IL($\pi\pi^*$) bands are not observed as this state is shifted to higher energies compared to the set of MLCT(phen) and MLCT(phz) states [1]. In this paper, we have synthesized a new polymeric complex, **P4VP-Re(dppz)**, in which the Re(CO)$_3$ core coordinating the dppz ligand is attached to the poly-4-vinyl-pyridine backbone by coordination of one third of the polymer's pyridines, corresponding to *ca.* 200 chromophores, **-[Re (CO)$_3$(dppz)**, per formula weight of the polymer, Scheme 1.

The complex was characterized by elemental analysis, FTIR and by TEM and AFM. Different conformations of a model monomer of **P4VP-Re(dppz)** were studied by computational methods in order to ascertain the effect of protonation over the molecular structure as well as over the absorption spectroscopy of **P4VP-Re(dppz)**. **P4VP-Re(dppz)** excited states and their redox reactivity towards the sacrificial reductant triethanolamine (TEOA) were studied by flash photolysis experiments either in DMF and in DMF/HClO$_4$. Those experiments were compared to the ones derived from thermal reactions of **P4VP-Re(dppz)** with solvated electrons in pulse radiolysis experiments. All the photophysical and photochemical properties studied were rationalized in terms of an interplay between ^{3}IL($\pi\pi^*$), ^{3}MLCT(phz) and the ^{3}MLCT(phen) states.

2. Material and methods

2.1. General

UV–vis spectra were recorded on a Shimadzu UV-1800 spectrophotometer. FTIR spectra were recorded on a Nicolet 8700 Thermo Scientific. Emission spectra were obtained with a computer-interfaced Near-IR Fluorolog-3 Research

Scheme 1. Structural formulae of P4VP-Re(dppz).

Spectrofluorometer. Spectra were corrected for differences in spectral response and light scattering. Solutions were deaereated with O$_2$-free nitrogen in a gas-tight apparatus before recording the spectra.

2.2. Synthesis

2.2.1. Dipyridil[3,2-a:2′3′-c]phenazine, dppz

The dppz was prepared by literature procedure [3,9,10]. 1,10-Phenanthroline-5,6-dione, 210 mg (1 mmol), and 1,2-Phenylendiamine, 130 mg (1.2 mmol), were suspended in 30 cm^3 of toluene and placed under an atmosphere of N$_2$. The mixture was heated to reflux, the reflux was maintained 2 h and it was then cooled to RT. The solid material was filtered by suction and dried under vacuum. The solid was recrystallized from EtOH until the UV–vis spectrum of the pure compound agreed well with the literature spectra. Yield 70%.

2.2.2. fac-[Re(CO)$_3$(dppz)Cl]

An equimolar mixture of Re(CO)$_5$Cl, 362 mg (1 mmol), and dppz, 282 mg (1 mmol), in 20 cm^3 of toluene under a N$_2$ atmosphere was refluxed for 3 h. The yellow–orange solid, *fac*-[Re(CO)$_3$(dppz)Cl], was recrystallized from EtOH. Yield 80%

2.2.3. fac-[Re(CO)$_3$(dppz)CF$_3$SO$_3$]

Equimolar amounts of *fac*-[Re(CO)$_3$(dppz)Cl], 470 mg (0.8 mmol) and AgCF$_3$SO$_3$, 206 mg (0.8 mmol) were dissolved in CH$_2$Cl$_2$. The solution was heated to reflux for 8 h under a N$_2$ atmosphere. The reaction mixture was left to reach RT and the solid formed during the reaction was filtered out. The mother liquor was rotovaporated to dryness. The yellow solid was recrystallized from CH$_2$Cl$_2$ by the addition of isooctane until the UV–vis spectrum of the pure compound agreed well with the literature spectra. Yield: 70%. FTIR (carbonyl stretching region, cm^{-1}): 2034.6, 1915,0. (See Fig. S1)

2.2.4. P4VP-Re(dppz)

To a solution containing 150 mg of poly-4-vinyl-pyridine (0.0025 mmol) in 100 cm^3 of CH$_2$Cl$_2$ were added 350 mg of Re (CO)$_3$(dppz)CF$_3$SO$_3$ (0.5 mmol) in 50 cm^3 of CH$_2$Cl$_2$. The liquid was stirred all through the addition of Re(CO)$_3$(dppz)CF$_3$SO$_3$. This stoichiometric relationship makes 200 Re(CO)$_3$(dppz)CF$_3$SO$_3$ react with a similar number of pyridine groups of the ca. 600 present in the polymer. A yellow solid precipitated during the 9 h that the solution was refluxed under a blanket of N$_2$. The mixture was rotoevaporated to dryness; the resulting solid was redissolved in the minimum volume of CH$_3$CN, and the polymer was precipitated by the slow addition of ethyl ether. Yield 75%. EA. Calcd. for {[(CH$_2$-CH-C$_5$H$_4$N)$_2$-(CH$_2$-CH-C$_5$H$_4$N)Re(CO)$_3$(C$_{18}$N$_4$H$_{10}$)]CF$_3$SO$_3$}$_{\sim200}$: C (50.78), N(9.64), H(3.07), S(3.15). Found: C(50.26), N(9.45), H (3.21), S(3.15) FTIR (carbonyl stretching region, cm^{-1}): 2032.6, 1916,9. Coordination of monomeric and polymeric pyridine ligands to metals have shown characteristic blue shifts for the in-plane CN stretching vibration of the pyridine ring by 15–20 wavenumbers relative to the CN stretch at 1598 cm^{-1} of uncoordinated pyridines [11]. The appearance of a new peak at 1616.08 cm^{-1} (absent in the FTIR spectra of both **P4VP** and *fac*-**[Re(CO)$_3$(dppz)CF$_3$SO$_3$]**) is consistent with the coordination of the pyridines to the Re(I) core in **P4VP-Re(dppz)** (See Fig. S1). The polymer **P4VP-Re(dppz)** and *fac*-**[Re(CO)$_3$(dppz)CF$_3$SO$_3$]** exhibited UV–vis spectra with similar features, but the extinction coefficients of the polymer, by comparison to the ones of *fac*-**[Re(CO)$_3$(dppz)CF$_3$SO$_3$]**, correspond to *ca.* 200 chromophores, **-[Re(CO)$_3$(dppz)**, per formula weight of the polymer. This load of Re(I) pendants was in good agreement with a calculation from the elemental analysis. The polymer is
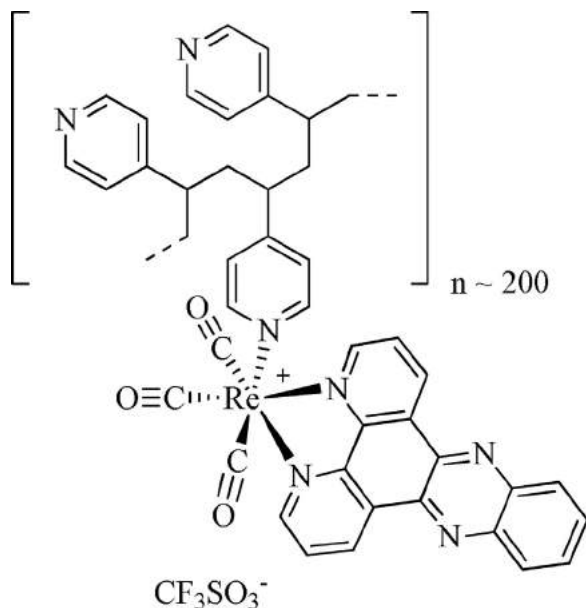
quite soluble in DMF but has a limited (very low) solubility in other organic solvents such as CH_2Cl_2 (DCM), MeOH, EtOH and MeCN.
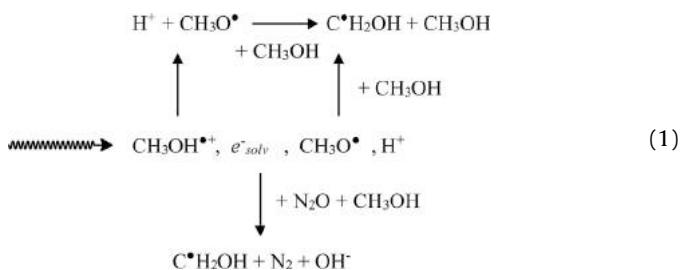
2.3. Photochemical measurements

Transient absorption spectra were performed by excitation with a Lambda Physik SLL-200 excimer laser (25 ns FWHM and 20–30 mJ/pulse at 351 nm), for transient absorption studies, the excitation beam was at a right angle with the white-light monitoring beam provided by a 1000-W Xe arc lamp probe source. The light was passed through a monochromator (PTI-1695) and detected by a Hamamatsu R758 photomultiplier. Decays typically represented the average of 10 to 30 pulses and were collected on a HP-54600B digital oscilloscope interfaced with a PC computer. Solutions for the photochemical work were deoxygenated with streams of ultrahigh-purity N_2 before and during the irradiations. A flow system ensured that the fresh solution was brought to the reaction cell in experiments where the decomposition of the Re(I) complexes and/or formation of products interfered with the optical measurements. The concentrations of the complexes were adjusted to provide homogeneous concentrations of the photogenerated intermediates within the volume of the irradiated solution, i.e., optical densities equal to or less than 0.1 (optical length = 1 cm) at 351 nm.

2.4. Pulse radiolysis

Pulse radiolysis experiments were carried out with a model TB-8/16-1S electron linear accelerator. The instrument and computerized data collection for time-resolved UV–vis spectroscopy and reaction kinetics have been described elsewhere [12,13]. Thiocyanate dosimetry was carried out at the beginning of each experimental session. Details of the dosimetry have been reported elsewhere [13,14]. The procedure is based on the concentration of $(SCN)_2^{\bullet-}$ radicals generated by the electron pulse in a N_2O-saturated 10^{-2} M SCN^- solution. In the procedure, the calculations were made with G = 6.13 and an extinction coefficient $\varepsilon = 7.58 \times 10^3$ M^{-1} cm^{-1} at 472 nm [13,14] for the $(SCN)_2^{\bullet-}$ radicals. In general, the experiments were carried out with doses that in N_2-saturated aqueous solutions resulted in $(1.7 \pm 0.1) \times 10^{-6}$ M to $(6.0 \pm 0.3) \times 10^{-6}$ M concentrations of e^-_{aq}. In these experiments, solutions were deaerated with streams of N_2 or N_2O gasses. In order to irradiate a fresh sample with each pulse, an appropriate flow of the solution through the reaction cell was maintained during the experiment.

The radiolysis of CH_3OH and CH_3OH/H_2O mixtures with ionizing radiation has been reported elsewhere in the literature [15–17]. These studies have shown that pulse radiolysis can be used as a convenient source of e^-_{solv} and $C^\bullet H_2OH$ radicals according to Eq.

$$H^+ + CH_3O^\bullet \longrightarrow C^\bullet H_2OH + CH_3OH$$
$$+ CH_3OH \qquad\qquad + CH_3OH$$
$$\uparrow \qquad\qquad\qquad \uparrow$$
$$\text{wwwww} \rightarrow CH_3OH^{\bullet+},\ e^-_{solv},\ CH_3O^\bullet,\ H^+ \qquad (1)$$
$$\downarrow + N_2O + CH_3OH$$
$$C^\bullet H_2OH + N_2 + OH^-$$

Thus, the main reducing species in pulse radiolysis of methanolic solutions under a N_2 atmosphere are e^-_{solv} and $C^\bullet H_2OH$. Since the latter species have large reduction potentials, i.e., -2.8 V vs. NHE for e^-_{solv} and -0.92 V vs. NHE for $C^\bullet H_2OH$, they have been used for the reduction of coordination complexes and for the study of electron transfer reactions. The yield of e^-_{solv} in CH_3OH (G ≈ 1.2) is about one third of the G-value in the radiolysis of H_2O (G ≈ 2.8) [15]. In solutions where e^-_{sol} was scavenged with N_2O [17], the $C^\bullet H_2OH$ radical appears to be the predominant product (yield >90%) of the reaction between CH_3OH and $O^{\bullet-}$.

2.5. TEM

Transmission electron micrographs (TEM) were recorded on a Philips EM 301 electron microscope at an electron acceleration voltage of 60 kV. Formvar stabilized with Carbon, 300 mesh, Copper approx. grid hole size 63 μm were used as grids for supporting polymer films. TEM images of **P4VP-Re(dppz)** polymer films were prepared with [Re(I)] = 2×10^{-5} M.

2.6. AFM

Formation of the Re(I) polymer aggregates from neat DCM, DMF or $HClO_4$/solvent solutions was monitored by Atomic Force Microscopy (AFM). In all the experiments, the concentration of the polymer was adjusted, in chromophore units, to [Re(I)] = 1 $\times 10^{-6}$ M, and a 10 μl aliquot was spotted stepwise on freshly cleaved Si substrates. After, the sample was dried under N_2. All images were obtained in ambient conditions. AFM measurements were performed in tapping mode, using a Multimode AFM with a nanoscope V controller (Bruker AXS, Santa Barbara, CA), equipped with a J-Scanner. Antimony (n) doped Si Cantilevers (T: 3.8 μm) with a nominal spring constant of 42 N/m (Bruker, model: TESP-V2) and f_0: 320 kHz were used. Five magnifications were taken by sample (10 μm × 10 μm, 5 μm × 5 μm, 2.5 μm × 2.5 μm, 1 μm × 1 μm and 0.3 μm × 0.3 μm).

2.7. Computational methods

Density Functional Theory (DFT) and Time Dependent Density Functional Theory (TD-DFT) calculations of ground and excited state properties of a series of Re(I) tricarbonyl complexes have been recently employed to interpret the experimental absorption bands arisen from a set of MLCT, LLCT and IL transitions [18–27]. The electronic structure of the Re(I) tricarbonyl complex were determined using tools of DFT [28–30] as implemented in Gaussian 09 package [31]. The optimization of the ground state geometry was carried out by means of the three-parameter hybrid functional developed by Becke [32] in conjunction with the LYP [33] exchange potential (B3LYP) with the LanL2DZ basis set which uses Dunning D95V basis set on C, N, O, H [34] and Los Alamos ECP plus DZ on Re [35–37]. Vibrational frequencies were computed at the same level of theory to confirm that these structures were minima on the energy surfaces. The vertical transition energies were calculated at the optimized ground-state geometry by TD-DFT [38–40] at the same level of theory. Both optimized geometries and TD-DFT calculations were carried out including solvent effects (DMF) through the Polarizable Continuum Model [41–43] to produce a number of 110 singlet-to-singlet transitions.

3. Results and discussion

New structural and reactive (thermal and photochemical) features are encompassed in the experimental observations presented and discussed in the separated sections below.

3.1. Polymer morphology: TEM and AFM observations

The morphologies of the polymer **P4VP-Re(dppz)** under different experimental conditions were studied by Transmission Electron Microscopy (TEM) and Atomic Force Microscopy (AFM). When taking micrographs, the films were not stained with any chemicals, and the contrast of the image in the TEM micrographs can only originate from the rhenium complexes incorporated to the polymers. All the cast films were obtained by slow evaporation of polymer solutions ($[Re] = 2 \times 10^{-5}$ M) over Formvar grids. Figs. 1–3 show the morphologies of the aggregates obtained from DMF, DMF/HClO$_4$ (0.05 M) and DCM cast films. In DMF, Fig. 1, vesicles were clearly observed from aggregation of **P4VP-Re(dppz)** strands. The vesicular nature is evidenced by a higher transmission in the center of the aggregates than around their periphery in the TEM pictures. Since contrast on TEM images arises from the metal centers, it is evident that in DMF the polymer strands are arranged with the Re(I) chromophores pointing to the interior of the vesicles and the uncoordinated pyridines of poly-4-vinyl-pyridine directed to the periphery. The sizes of the vesicles outer diameters range from 140 to 220 nm, *i.e.* they are not very polydisperse. Since other previously studied Re(I) polymers tend to form highly polydisperse aggregates [44–46], this greatly diminished polydispersity is a new and interesting feature of the **P4VP-Re(dppz)** polymer.

In DMF/HClO$_4$ (0.05 M), Fig. 2, the **P4VP-Re(dppz)** strands tend to aggregate into small spherical nanodomains (top panel) with

outer diameters ranging from 8 to 40 nm. However, large compound vesicles, ranging from 300 to 700 nm in diameter, were also observed (bottom panel).

Therefore, protonation of free pyridines as well as **-Re(CO)$_3$(dppz)$^+$** chromophores tend to break the vesicles into smaller aggregates in addition to the formation of LCV. In DCM, Fig. 3, the **P4VP-Re(dppz)** strands tend to aggregate into medium size spherical nanodomains with outer diameters ranging from 60 to 110 nm.

Samples were loaded onto a Si surface and observed under AFM to further characterize the morphologies of the aggregates formed by **P4VP-Re(dppz)** under different experimental conditions. The dimensions of the oligomers were estimated by measuring their heights with the use of the Gwyddion free-software. Fig. 4 show AFM images on cast films obtained from **P4VP-Re(dppz)** in DCM (Fig. 4A) and in HClO$_4$/DCM (Fig. 4B). Fig. 5 shows AFM images on cast films obtained from **P4VP-Re(dppz)** in DMF (Fig. 5A) and in HClO$_4$/DMF (Fig. 5B).

P4VP-Re(dppz) in DCM (Fig. 4) was characterized by aggregates forming rings all over the surface, even at magnifications of 50 μm × 50 μm. Those rings have diameters varying from 300 to 700 nm and a maximum height of 10 nm (both measured from their rugosity profiles). Those rings are formed by small pearl-shape particles with diameters of ∼60–70 nm and heights around 10 nm. In addition to the rings, very small (*i.e.* at polymer scales) spherical objects with diameters of a few nm are observed. Fig. 4B
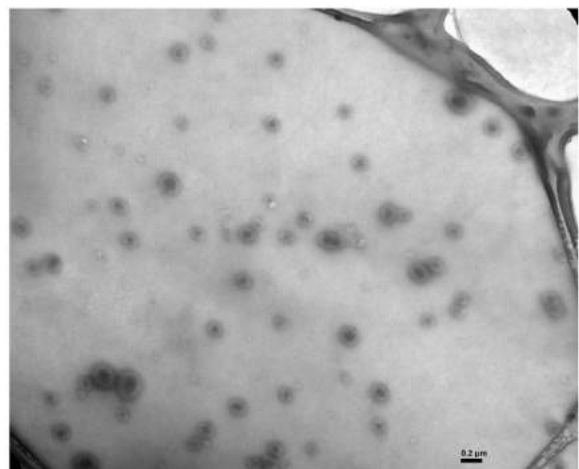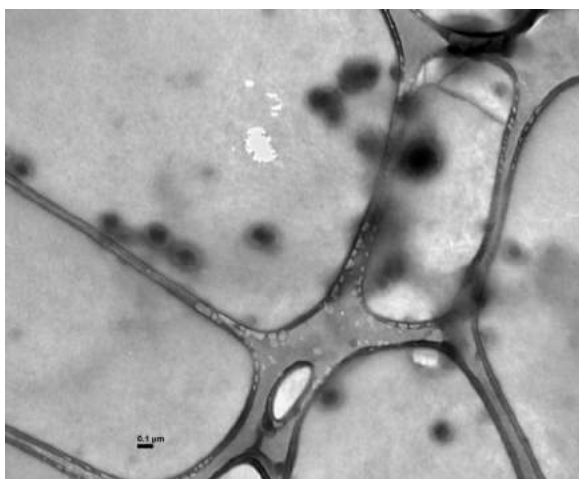
Fig. 1. TEM images of **P4VP-Re(dppz)** polymer films prepared with $[Re(I)] = 2 \times 10^{-5}$ M in DMF. See text for details.
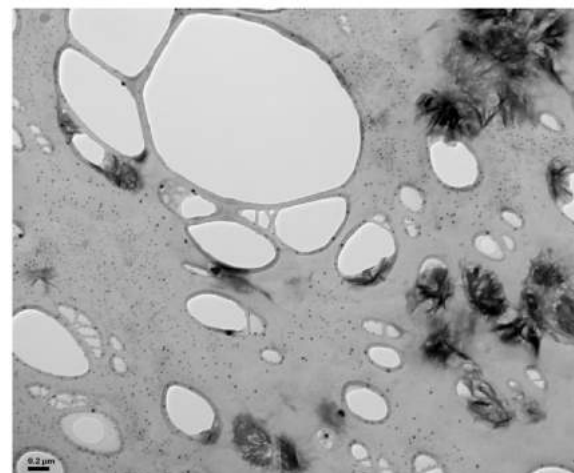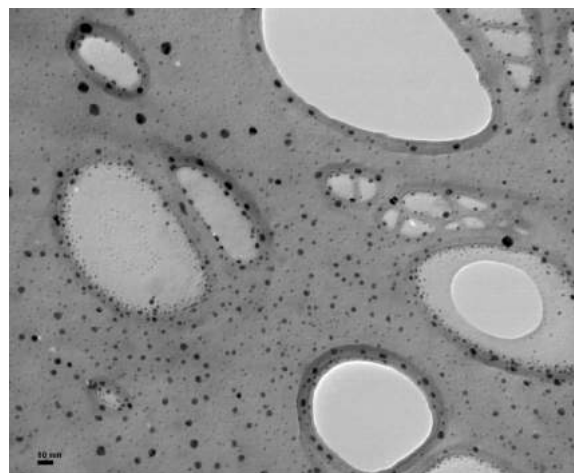
Fig. 2. TEM images of **P4VP-Re(dppz)** polymer films prepared with $[Re(I)] = 2 \times 10^{-5}$ M in DMF/HClO$_4$. See text for details.

shows that in HClO$_4$/DCM the morphology of **P4VP-Re(dppz)** is profoundly altered. It can be observed over the scanned surface that the ring-type structures have disappeared, though the small pearl-shape particles which were forming the rings in neat DCM are still present in HClO$_4$/DCM. This morphology is characterized by a non-homogeneous spreading of oligomers with a bimodal distribution of sizes: one distribution is formed by particles with diameters of $\sim 150 \pm 50$ nm and heights around 10 nm while the other one consists of particles with diameters of $\sim 50 \pm 20$ nm and heights below 5 nm.

Fig. 5A shows AFM images of **P4VP-Re(dppz)** in DMF. In this condition particles without definite shapes were observed over the substrate, with sizes which span between 50 ± 30 nm and 400 ± 300 nm. In some of the cases aggregation of those particles is observed forming islands up to 1 μm in width. The height of these kind of particles is between 3 and 15 nm.

In HClO$_4$/DMF pyramidal like particles were observed over the scanned surface, with dimensions of 1 μm of base and a height of 20 nm. These pyramidal structures present another type of particle over their surface, with a much more rounded shape, of about ~ 100 nm (diameter) and 3 nm (height). Phase-analysis of these images show that pyramids and spherical particles have different contrast in the phase, therefore it can be inferred that both type of structures consist of different chemical composition. In co-existence with those pyramidal structures there are spherical particles with diameters ~ 400 nm and heights of 60 nm.

Due to the different experimental requirements of AFM and TEM techniques, the concentration of the polymer used for AFM studies was [Re(I)] = 1×10^{-6} M in contrast to [Re(I)] = 2×10^{-5} M which was used in TEM experiments. Therefore, AFM studies reflect the morphology of polymer aggregates in a much more diluted (20-fold) regime than TEM studies. Interestingly, the formation of rings, evidenced in AFM/DCM experiments, was not observed in TEM studies in the same solvent. Those rings are composed of pearled like particles. It seems that at the 20-fold higher concentration used in TEM studies than in AFM studies, the aggregates tend to come close together and the formation of any other structure like the rings observed at much diluted concentrations is precluded. In DMF, the morphology of **P4VP-Re(dppz)** is somewhat different as seen from TEM or AFM spectroscopies. TEM studies show, in neat DMF, the formation of vesicles of low polydispersity while AFM images show a non-homogeneous distribution of oligomers showing distorted spherical islands. It seems that the formation of vesicles is a concentration dependent morphological phenomenon. However, after protonation, those

vesicles are not observed any more by TEM. AFM shows, however, the formation of pyramidal structures in co-existence with spherical objects.

3.2. Photophysical and photochemical properties

3.2.1. Origins of the absorption spectroscopy of fac-XRe(CO)$_3$L complexes

Ligand-field (LF), metal-to-ligand charge transfer (MLCT), ligand-to-ligand charge transfer (LLCT), and intra-ligand (IL) transitions have been invoked to interpret the lowest energy absorption bands of *fac*-XRe(CO)$_3$L complexes which occur in the near-UV region. Usually, CT bands ($\lambda_{max} \sim 330$–400 nm; $\varepsilon \sim (2$–$5) \times 10^3$ M^{-1} cm^{-1}) appear to some extent at longer wavelengths than the more intense IL bands ($\lambda_{max} \sim 240$–320 nm with $\varepsilon \sim 2 \times 10^4$ M^{-1} cm^{-1}) [47]. The correctness of these simplified models have been examined by recent TD-DFT studies in [Re(bpy)(CO)$_3$Cl] and [Re(bpy)(CO)$_3$(py)]$^+$ complexes (bpy = 2,2′bipyridine, py = pyridine). For example, in the former the HOMO can be described as containing more than 50% of Re character, with contributions of around 20% each from CO and Cl. However, the LUMO is composed of more than 80% of bpy character [48]. The lowest energy optical transition can be assigned as having metal-ligand-to-ligand charge transfer (MLLCT) character rather than a pure MLCT. In addition, we have recently performed TD-DFT calculations on two related water soluble Re(I) complexes which showed also that their lowest energy absorption bands can be described as having MLLCT character [49,50]. LLCT excited states generally occur in complexes bearing both reducing (D) and oxidizing (A) type of ligands as a result of a charge transfer from one donor ligand to an acceptor ligand. Lowest excited states of a LLCT character have been observed in several examples of Re(I)-tricarbonyl complexes [48]. In those complexes, the very weak electronic interactions between D-A make the extinction coefficients of LLCT bands very low. As a result, LLCT transitions are not usually observed directly from absorbance UV–vis spectroscopy as it is usually done with MLCT transitions. Moreover, as in general LLCT states are non-emissive, their excited-state characteristics can be studied only by transient spectroscopy [48]. Due to the last observations, LLCT states are usually elusive when compared to MLCT states.

3.2.2. DFT and TD-DFT calculations

The geometry of a fraction of the Re polymer, hereafter named **(py)$_3$-Redppz$^+$**, consisting of 3 pyridines (one of them coordinated to the Re(CO)$_3$(dppz) chromophore) was optimized at the B3LYP/LanL2dZ (in vacuo) level of theory. In the optimized structure of **(py)$_3$-Redppz$^+$**, calculated Re-N(dppz) distances of 2.186 and 2.187 Å and Re-N(py) distance of 2.233 Å are in good agreement to the experimental and calculated ones for [Re(CO)$_3$(dppzBr)(py)] PF$_6$ [7], which provide a good method of validating these calculations. The structures of other three possible protonated species, *i.e.* **(pyH)$_2$-pyRedppz^{3+}**, **(pyH)$_2$-pyRedppzH^{4+}** and **(pyH)$_2$-pyRedppzH$_2$$^{5+}$**, were also optimized at the same level of theory, see Fig. 6.

In **(py)$_3$-Redppz$^+$** the two free pyridines lie in a stacking arrange. However, in **(pyH)$_2$-pyRedppz^{3+}** the protonated pyridines tend to separate apart. In fact, dihedral C-C-C-C angles adjacent to the pyridines are 83.6^0 and -62.0^0 in **(py)$_3$-Redppz$^+$** while the same dihedral angles correspond to 26.8^0 and -170.0^0 in **(pyH)$_2$-pyRedppz^{3+}**. In addition to the structural changes experienced by the poly-pyridine backbone upon protonation, protonation of dppz distorts the ligand from a planar structure and also shifts the dppz from being in the equatorial plane of the molecule. The distortion of the dppz ligand from planarity after electron reduction followed by protonation has been previously observed in DFT calculations on the dppz ligand [51]. To a certain extent, in the sense that an
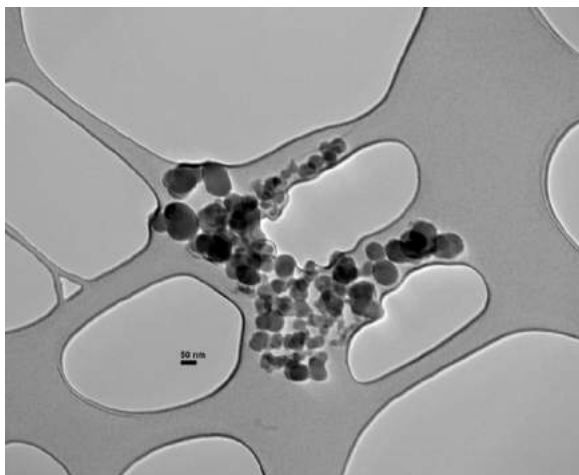

Fig. 3. TEM images of **P4VP-Re(dppz)** polymer films prepared with [Re(I)] = 2×10^{-5} M in DCM. See text for details.
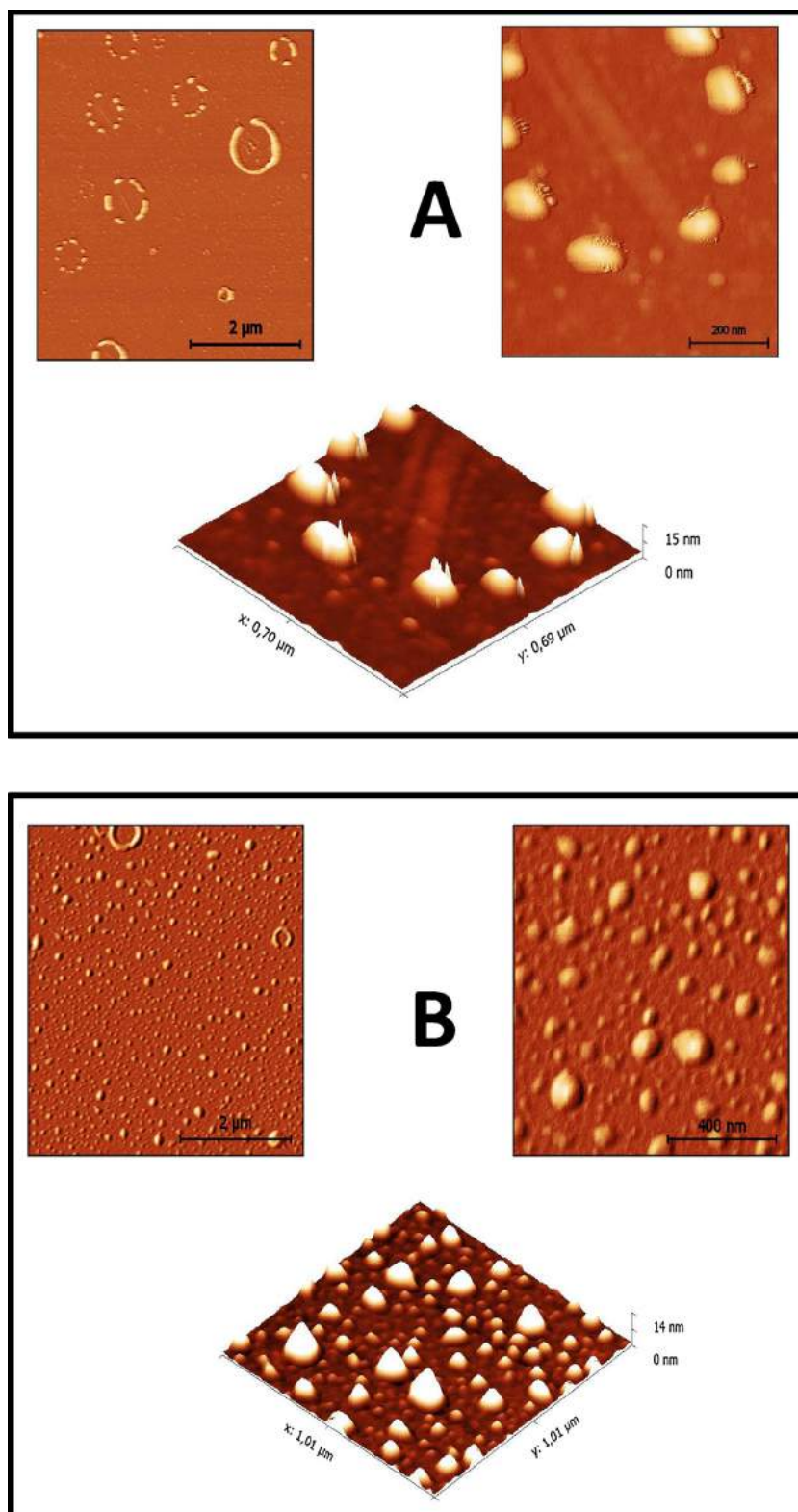
Fig. 4. AFM images for **P4VP-Re(dppz)** in DCM (top panel A) and DCM/HClO$_4$ 0.05 M (bottom panel B).

expansion of the poly-vinylpyridine backbone is predicted after protonation, DFT calculations on **(py)$_3$-Redppz$^+$**, **(pyH)$_2$-pyRedppz^{3+}**, **(pyH)$_2$-pyRedppzH^{4+}** and **(pyH)$_2$-pyRedppzH$_2$$^{5+}$** are in

agreement with the TEM observations communicated above in Figs. 1 and 2.

TD-DFT calculations were performed on the different geometry optimized structures described above to better understand the
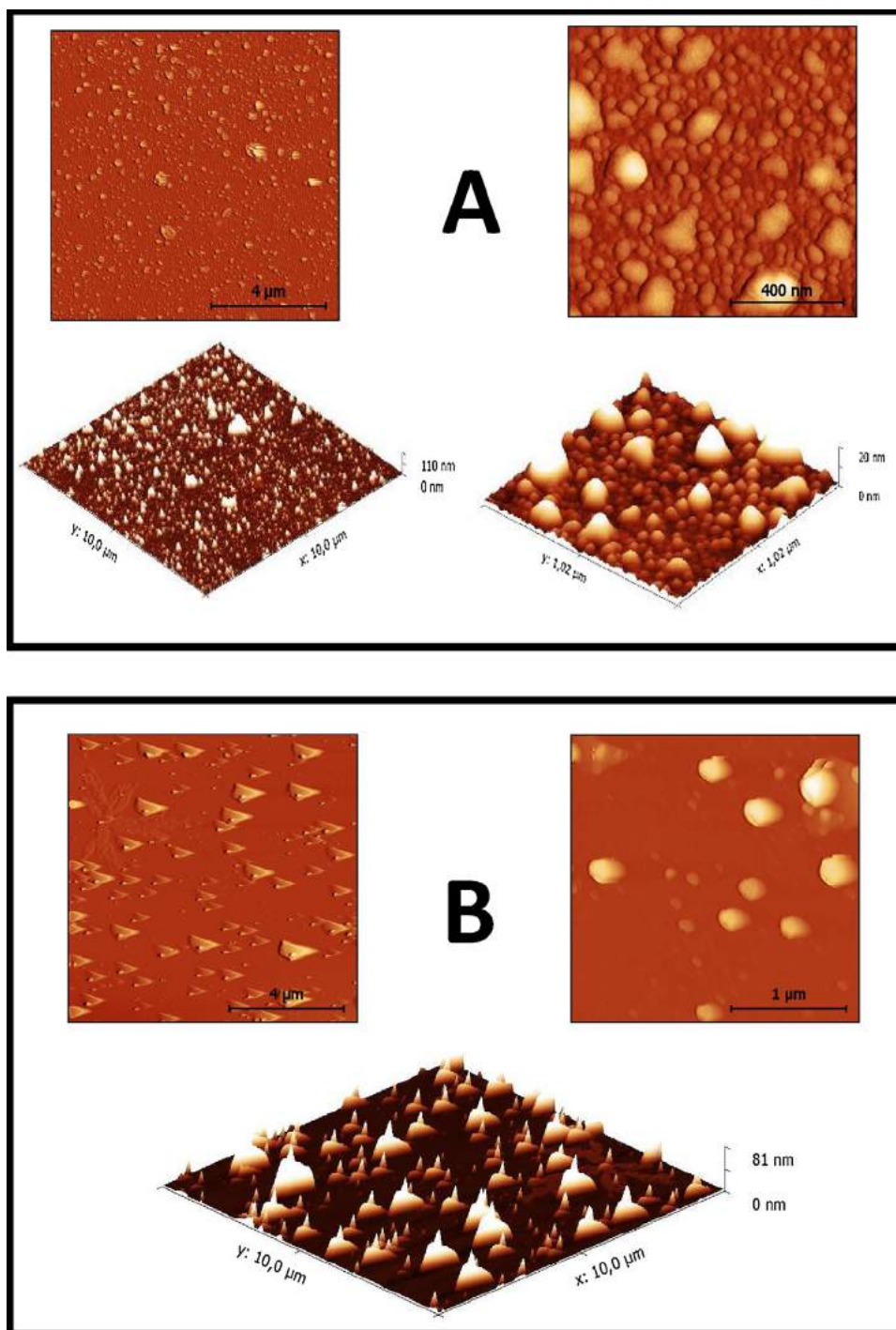
Fig. 5. AFM images for **P4VP-Re(dppz)** in DMF (top panel **A**) and DMF/HClO$_4$ 0.05 M (bottom panel **B**).

medium effects on the photophysical properties of the Re(I) complex. In the following section, TD-DFT results corresponding to the lowest energy bands of the Re(I) complexes will be discussed in detail, as the electronic transitions in this near UV–vis energy region are the ones responsible of the observed photophysical and photochemical properties of **P4VP-Re(dppz)** when exciting with photonic energies corresponding to λ_{exc} = 350 nm.

The lowest energy singlet-singlet electronic transitions calculated for **(py)$_3$-Redppz$^+$**, **(pyH)$_2$-pyRedppz^{3+}** and **(pyH)$_2$-pyRedppzH^{4+}** at their optimized structures consist of H → L for both **(py)$_3$-Redppz$^+$** and **(pyH)$_2$-pyRedppz^{3+}** and H → L + 1 for **(pyH)$_2$-pyRedppzH^{4+}**. Fig. 7 shows the experimental absorption spectra of

P4VP-Re(dppz) in DMF and DMF/HClO$_4$ (0.05 M) as well as the calculated oscillator strengths for **(py)$_3$-Redppz$^+$**, **(pyH)$_2$-pyRedppz^{3+}** and **(pyH)$_2$-pyRedppzH^{4+}** at the B3LYP/LanL2DZ/PCM/DMF level of theory.

Oscillator strengths follow the experimental absorption bands in the UV–vis spectral region with a reasonable precision in both position and relative intensities. There is a red shift, relative to the experimental absorption spectra, of the calculated oscillator strengths of about 25 nm. This discrepancy is typical of TD-DFT calculations on coordination compounds. Fig. 8 shows an energy level diagram of the frontier MOs of **(py)$_3$-Redppz$^+$**, **(pyH)$_2$-pyRedppz^{3+}**,**(pyH)$_2$-pyRedppzH^{4+}**and   **(pyH)$_2$-pyRedppzH$_2$$^{5+}$**

Fig. 6. Optimized GS structures for **(py)₃-Redppz⁺**, **(pyH)₂-pyRedppz³⁺**, **(pyH)₂-pyRedppzH⁴⁺** and **(pyH)₂-pyRedppzH₂⁵⁺**.

along with spatial plots of **(py)₃-Redppz⁺** MOs which describe its spectroscopy in the 300–400 nm region (see Tables 1 and 2 for a description of the calculated wavelengths, oscillator strengths and major MO configurations).
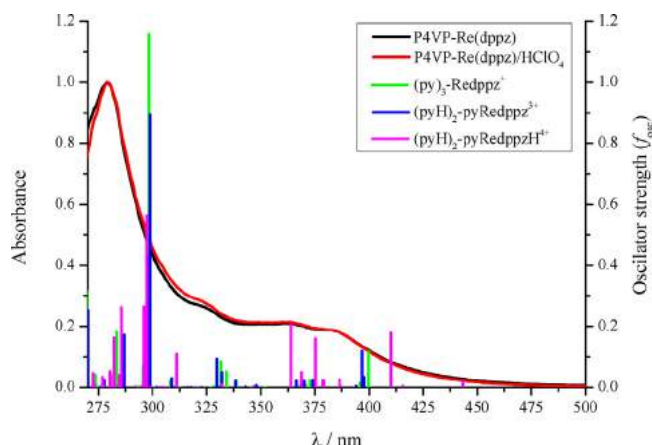
Figs. S1–S3 and Tables S1–S4 shows spatial plots of the most representative MOs, the calculated wavelengths, oscillator strengths and major MO configurations for **(py)₃-Redppz⁺**, **(pyH)₂-pyRedppz³⁺**, **(pyH)₂-pyRedppzH⁴⁺** and **(pyH)₂-pyR-edppzH₂⁵⁺** in the 235–450 nm spectral range.

For **(py)₃-Redppz⁺**, H and H-1 are MOs mainly metal based $(d\pi)$ which contain significant CO (π^*) character from the CO ligands, with some contribution of the axial py ligand in H and no contribution from this axial ligand in H-1. H-3 is a MO centered on the dppz ligand with higher electron density residing on the phz portion than in the phen portion of it. H-10 is a MO mostly centered on the phz portion of dppz. L, L + 1 and L + 2 are MOs which can be assigned to dppz b1(phz), dppz b1(phen) and dppz a2 LUMOs of dppz as described by van der Salm et al. [7]. In the following discussion we have used a prime (as in a2′) for a LUMO of dppz which is similar but not exactly the same of the ones described by van der Salm et al. In addition, dppz(1) and dppz(2) imply different HOMOs of dppz. It is observed that after protonation of dppz, L is stabilized and H-L energy gap decreases.
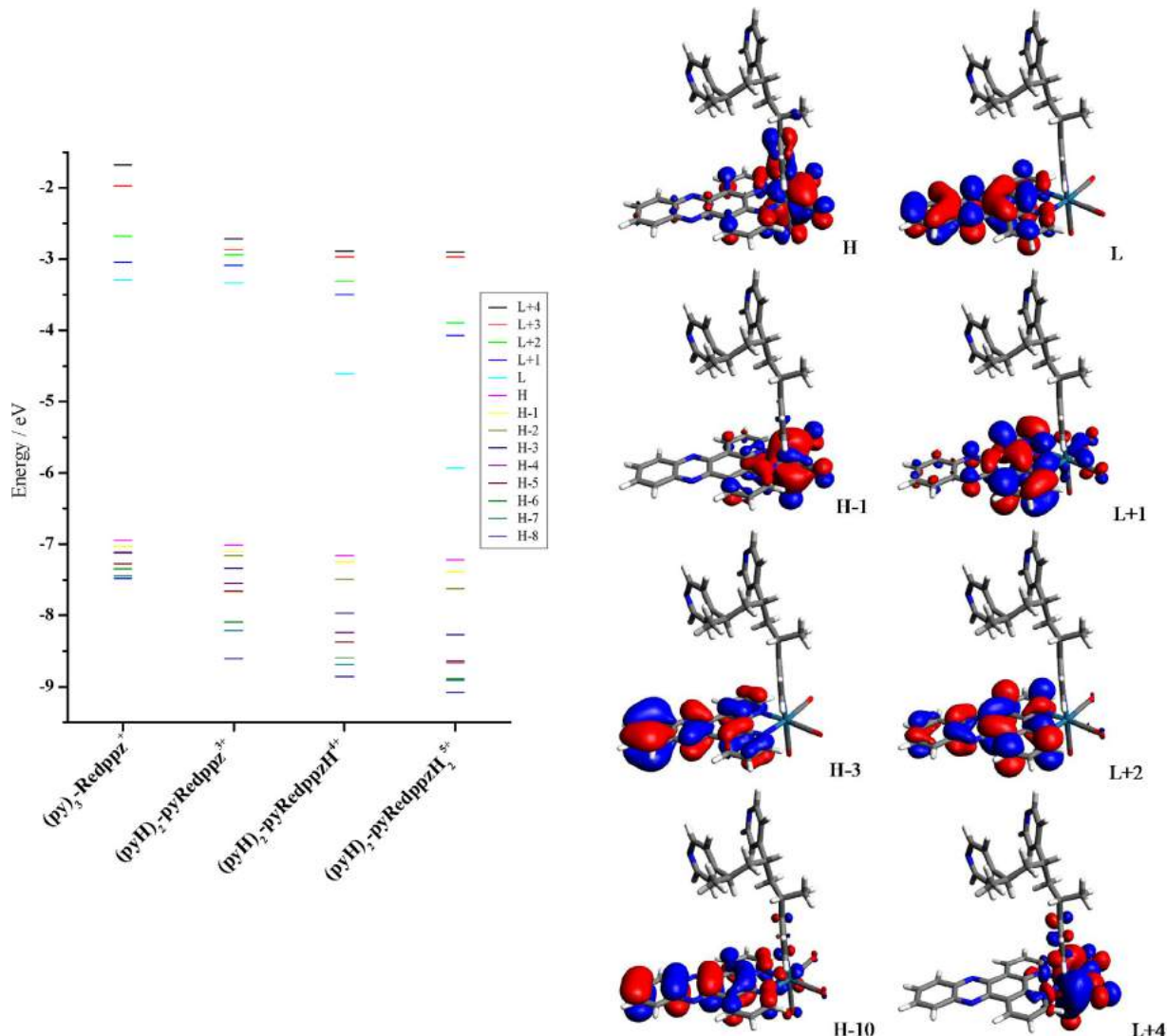
The spectroscopy in the 300–400 nm region for **(py)₃-Redppz⁺**, **(pyH)₂-pyRedppz³⁺**,**(pyH)₂-pyRedppzH⁴⁺**and **(pyH)₂-pyR-edppzH₂⁵⁺** can be described by a set of metal-ligand-to-ligand (MLLCT), intra-ligand (IL), ligand-to-ligand-charge-transfer (LLCT) and metal-centered (MC) electronic transitions. MLLCT transitions involve the transfer of charge density from pyRe(CO)₃ portion of the molecule to either the phenazine or phenanthroline part of the dppz (as in dppz b1(phz) or dppz b1(phen) LUMOs of dppz) or to a LUMO involving the whole dppz ligand (as in dppz a2), see Tables 1

Fig. 7. Comparison of the UV–vis absorption spectrum of **P4VP-Re(dppz)** in DMF and in DMF/HClO$_4$ 0.05 M (black and red lines, respectively) with TD-DFT calculated electronic transitions for **(py)$_3$-Redppz$^+$**, **(pyH)$_2$-pyRedppz^{3+}**, **(pyH)$_2$-pyRedppzH^{4+}** (f_{osc}, vertical lines). See text for details. (For interpretation of the references to color in this figure legend, the reader is referred to the web version of this article.)

and 2. We turn now to describe the protonation effect on the calculated spectroscopy of **(pyH)$_2$-pyRedppz^{3+}**, **(pyH)$_2$-pyRedppzH^{4+}** and **(pyH)$_2$-pyRedppzH$_2$$^{5+}$**. In passing from **(py)$_3$-Redppz$^+$** to **(pyH)$_2$-pyRedppz^{3+}** there are only minor differences in the calculated electronic transitions (i.e. λ_{calc} and the nature of the electronic transitions are very similar). However, some subtle differences can be pointed out. Firstly, the lowest energy band of **(pyH)$_2$-pyRedppz^{3+}** is composed of an IL (dppz phz → dppz b1 (phz)) transition in addition to the MLLCT(pyRe(CO)$_3$ → dppz b1 (phz)) and MLLCT(pyRe(CO)$_3$ → dppz b1(phen)) transitions which are the only present in the lowest energy band of **(py)$_3$-Redppz$^+$**. Secondly, MC (Re d-d) and MLCT (Re → py) transitions appear in the highest energy band of **(pyH)$_2$-pyRedppz^{3+}**). Single proton-ation of dppz in addition to protonation of the free pyridines (i.e. **(pyH)$_2$-pyRedppzH^{4+}**) shifts MLLCT(pyRe(CO)$_3$ → dppz b1(phen)) and MLLCT (pyRe(CO)$_3$ → dppz a2) to lower energies (compared to **(py)$_3$-Redppz$^+$** and/or **(pyH)$_2$-pyRedppz^{3+}**) and also places IL transitions close in energy to MLLCT ones. In addition, MLLCT(pyRe (CO)$_3$ → dppz b1(phz)) is higher in energy in **(pyH)$_2$-pyRedppzH^{4+}** than in **(py)$_3$-Redppz$^+$** or **(pyH)$_2$-pyRedppz^{3+}**. Protonation of both N of dppz brings into play LLCT transitions in addition to MLLCT

Fig. 8. Energy level diagram of the frontier MOs of **(py)$_3$-Redppz$^+$**, **(pyH)$_2$-pyRedppz^{3+}**, **(pyH)$_2$-pyRedppzH^{4+}** and **(pyH)$_2$-pyRedppzH$_2$$^{5+}$** along with spatial plots of **(py)$_3$-Redppz$^+$** MOs which describe its spectroscopy in the 300–400 nm region. See text for details.

Table 1
Main electronic transitions in the 300–400 nm region for **(py)₃-Redppz⁺** and **(pyH)₂-pyRedppz³⁺** at the B3LYP/LanL2DZ/PCM (DMF) level of theory .

λ_{calc}/nm	f_{osc}	Major MO configurations (% contribution)	Character
(py)₃-Redppz⁺			
399.7	0.1159	H → L (78%)	MLLCT(pyRe(CO)₃ → dppz b1(phz))
		H → L+1 (15%)	MLLCT(pyRe(CO)₃ → dppz b1(phen))
334.0	0.0514	H → L+2 (75%)	MLLCT (pyRe(CO)₃ → dppz a2)
		H-3 → L+1 (17%)	IL (dppz → dppz b1(phen)
331.6	0.0851	H-1 → L+2 (90%)	MLLCT (pyRe(CO)₃ → dppz a2)
298.3	1.1573	H-3 → L+2 (53%)	IL (dppz → dppz a2)
		H-10 → L (30%)	IL (dppz → dppz b1(phz))
(pyH)₂-pyRedppz³⁺			
396.8	0.1189	H → L (61%)	MLLCT(pyRe(CO)₃ → dppz b1(phz))
		H-4 → L (21%)	IL (dppz phz → dppz b1(phz))
		H → L+1 (12%)	MLLCT (pyRe(CO)₃ → dppz b1(phen))
332.1	0.0485	H → L+4 (80%)	MLLCT (pyRe(CO)₃ → dppz a2)
		H-2 → L+1 (12%)	IL (dppz → dppz b1(phen))
329.8	0.0935	H-1 → L+4 (91%)	MLLCT(pyRe(CO)₃ → dppz a2)
298.8	0.8937	H-2 → L+4 (38%)	IL (dppz → dppz a2)
		H-5 → L (21%)	IL (dppz → dppz b1(phz))
		H-1 → L+8 (15%)	MC (Re d-d)
		H → L+5 (14%)	MLCT (Re → py)

and IL transitions. In the DMF/0.05 M HClO₄ solutions, it is probable that the existing species may be polymer strands with the free pyridines fully protonated while some Re(I) chromophores may have either one or both protonated N in their dppz structure. Therefore, **(pyH)₂-pyRedppzH⁴⁺** and **(pyH)₂-pyRedppzH₂⁵⁺** may be our very rough approximation to the existing species in the actual solutions.

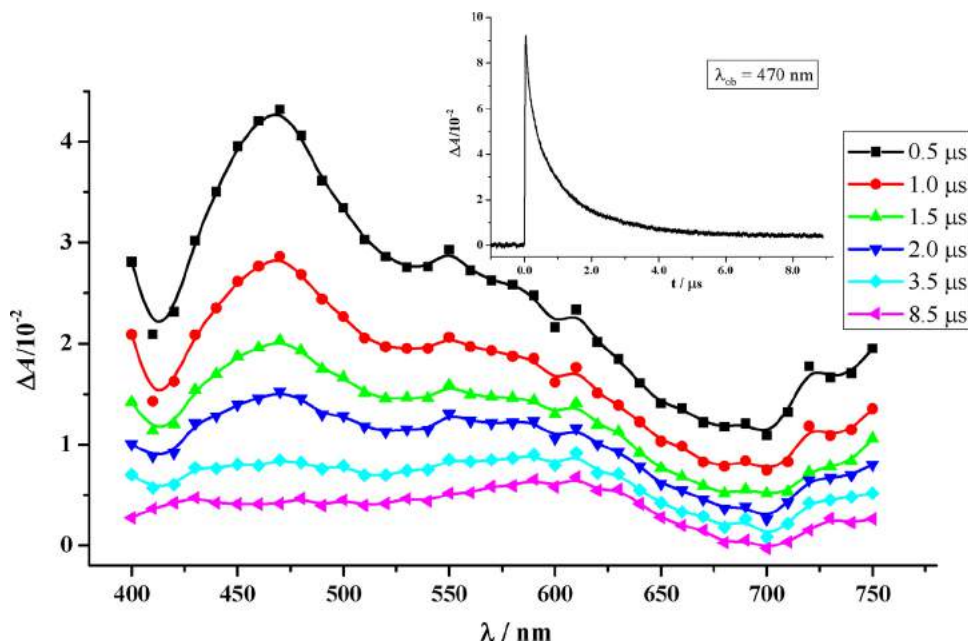### 3.2.3. Flash photochemical experiments

After optical excitation at 350 nm of a solution of **P4VP-Re (dppz)** ([Re] = 1 × 10⁻⁴ M) in deaereated DMF a weak luminescence was detected ($\Phi_{lum} < 1 \times 10^{-4}$). However, with the same solution in flash photolysis (FP) experiments, a transient absorbing at λ_{max} = 475, 500 and $\lambda > 750$ nm could be detected, see Fig. 9. A biexponential function with lifetimes $\tau_1 = 0.24 \pm 0.06\,\mu s$ and $\tau_2 = 1.5 \pm 0.2\,\mu s$ was fitted to oscillographic traces collected between λ_{obs} = 400 nm and λ_{obs} = 650 nm.

A transient of very similar spectral features was observed in FP experiments with **fac-[Re(CO)₃(dppz)CF₃SO₃]** in MeOH (see Fig. S5). The decay of this transient could only be fitted by a biexponential function with $\tau_1 = 0.54 \pm 0.06\,\mu s$ and $\tau_2 = 5.0 \pm 0.2\,\mu s$. The two lifetimes of **fac-[Re(CO)₃(dppz)CF₃SO₃]** determined in FP

Table 2
Main electronic transitions in the 300–400 nm region for (pyH)₂-pyRedppzH⁴⁺ and (pyH)₂-pyRedppzH₂⁵⁺ at the B3LYP/LanL2DZ/PCM (DMF) level of theory.

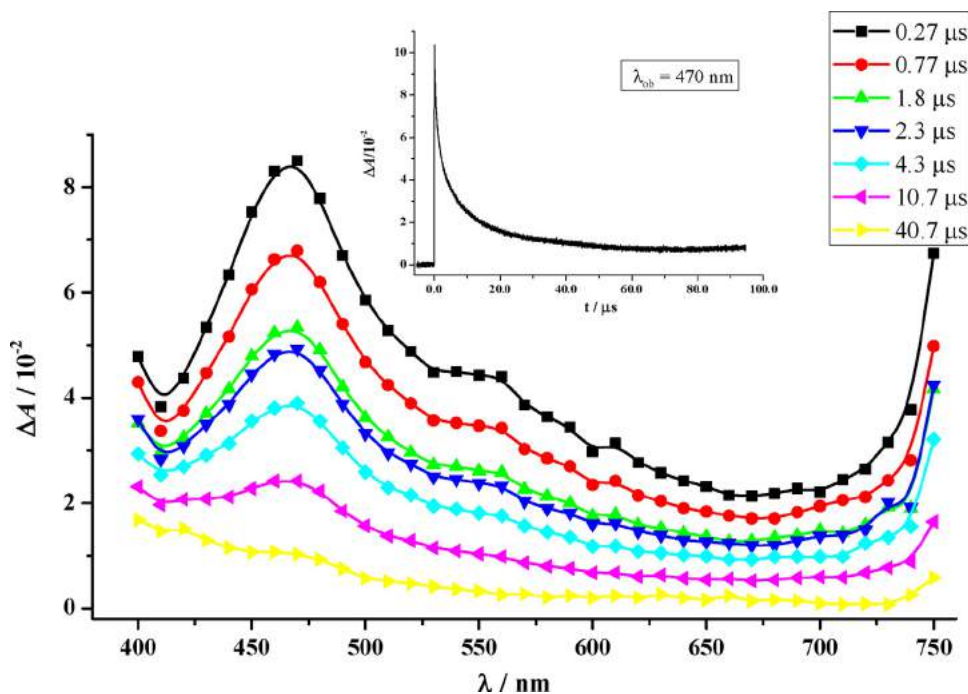| λ_{calc}/nm	f_{osc}	Major MO configurations (% contribution)	Character
(pyH)₂-pyRedppzH⁴⁺			
410.2	0.1789	H → L+1 (88%)	MLLCT(pyRe(CO)₃ → dppz b1(phen))
375.3	0.1597	H-5 → L (36%)	IL (dppz(1) → dppz b1(phz)
		H-6 → L (35%)	IL (dppz(2) → dppz b1(phz)
		H → L+2 (19%)	MLLCT (pyRe(CO)₃ → dppz a2)
368.8	0.0492	H-1 → L+2 (85%)	MLLCT(Re(CO)₃ → dppz a2)
311.1	0.1091	H-3 → L+1 (89%)	IL (dppz b1(phz) → dppz b1(phen))
297.3	0.5622	H-3 → L+2 (44%)	IL (dppz b1(phz) → dppz a2)
		H-5 → L+1 (12%)	IL (dppz(1) → dppz b1(phen))
		H-1 → L+8 (17%)	MC (Re d-d) + MLCT (Re → py, dppz b1(phz))
(pyH)₂-pyRedppzH₂⁵⁺			
468.8	0.0774	H → L+2 (63%)	MLLCT (pyRe(CO)₃ → dppz b1(phen))
		H-1 → L+2 (18%)	MLLCT (Re(CO)₃ → dppz b1(phen))
		H → L+1 (14%)	MLLCT (pyRe(CO)₃ → dppz a2)
444.3	0.1809	H-1 → L+2 (31%)	MLLCT (Re(CO)₃ → dppz b1(phen))
		H-7 → L (26%)	LLCT ((pyH)₂ → dppz b1(phz))
		H-1 → L+1 (18%)	MLLCT (Re(CO)₃ → dppz a2)
443.9	0.0623	H-7 → L (67%)	LLCT ((pyH)₂ → dppz b1(phz))
		H-1 → L+2 (13%)	MLLCT (Re(CO)₃ → dppz b1(phen))
427.6	0.4452	H-8 → L (57%)	LLCT ((pyH)₂ → dppz b1(phz)) + IL (dppz → dppz b1(phz)
		H-2 → L+2 (26%)	MLLCT (Re(CO)₃ → dppz b1(phen))
		H-9 → L (12%)	LLCT ((pyH)₂ → dppz b1(phz)) (12%)
306.4	0.7204	H-4 → L+1 (46%)	LLCT (py → dppz a2) + IL(dppz → dppz a2)
		H → L+6 (22%)	MLLCT (pyRe(CO)₃ → dppz a2')
		H-5 → L+1 (10%)	LLCT (py → dppz a2)
302.1	0.1069	H → L+6 (33%)	MLLCT (pyRe(CO)₃ → dppz a2') (33%)
		H-4 → L+1 (16%)	LLCT (py → dppz a2)
		H-18 → L (16%)	LLCT ((CH₃)-CH-pyH⁺, py-HC(CH₃)-CH₂- → dppz b1(phz))

Fig. 9. Transient spectra recorded at different delays after the laser pulse in flash photolysis experiments of **P4VP-Re(dppz)** in deaerated DMF. Inset show an oscilographic trace at λ_{ob} = 470. See text for details.

experiments are very similar to those observed for the ^{3}IL($\pi\pi^*$) in **fac-[Re(CO)$_3$(dppz)py]$^+$**, *i.e.* τ_1 = 0.5 μs and τ_2 = 3.5 μs, determined by TRIR [52], suggesting that the spectra of Fig. S5 can be assigned to the ^{3}IL($\pi\pi^*$) decaying by non-radiative processes. The similarity between the transient spectra in FP experiments of **fac-[Re(CO)$_3$(dppz)CF$_3$SO$_3$]** and **P4VP-Re(dppz)** suggests that the ^{3}IL($\pi\pi^*$) is the dominant species in both systems decaying by a bi-exponential regime. Though a longer lifetime for **fac-[Re(CO)$_3$(dppz)CF$_3$SO$_3$]** than for **P4VP-Re(dppz)** could be associated with the availability of new deactivation pathways for the ^{3}IL($\pi\pi^*$)

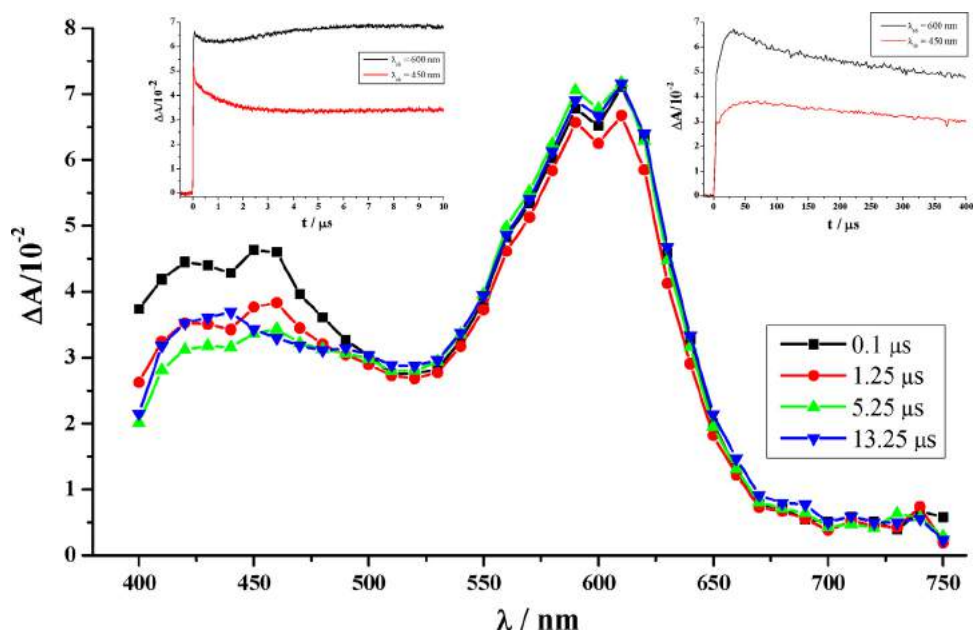in the polymer due to vibration modes present in the poly-4-vinyl-pyridine backbone.

When FP experiments were carried out with a solution of **P4VP-Re(dppz)** ([Re] = 1 × 10^{-4} M) in DMF/HClO$_4$ 0.05 M a transient with similar absorption features to the transient of Fig. 9 was observed, see Fig. 10.

However, the nonradiative decay of the transient recorded in FP experiments under HClO$_4$ 0.05 M, albeit being bi-exponential, was much slower than in FP experiments in the absence of HClO$_4$ acid, with lifetimes of τ_{1H^+} = 1.6 ± 0.2 μs and τ_{2H^+} = 15 ± 1 μs. In fact, τ_2

Fig. 10. Transient spectra recorded at different delays after the laser pulse in flash photolysis experiments of **P4VP-Re(dppz)** in deaerated DFM/HClO$_4$ 0.05 M. Inset show an oscilographic trace at λ_{ob} = 470. See text for details.
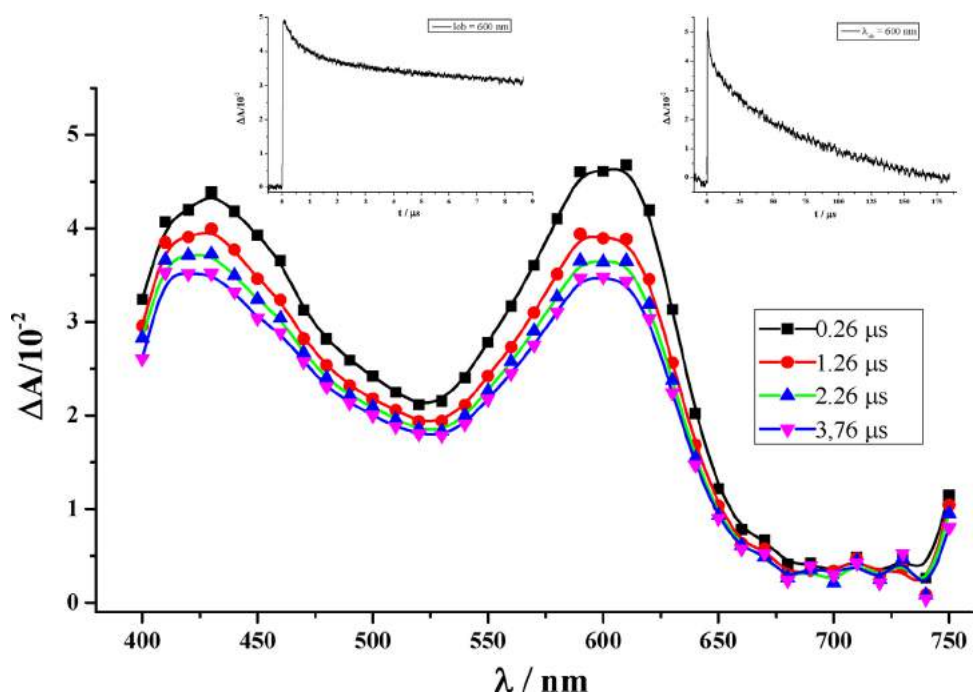
Fig. 11. Transient spectra recorded at different delays after the laser pulse in flash photolysis experiments of **P4VP-Re(dppz)** in deaerated DFM containing TEOA 0.075 M. Insets show oscilographic traces at λ_{ob} = 450 and 600 nm in the 0–10 μs time range (left panel) and in the 0–400 μs time range (right panel). See text for details.

$\sim\tau_{1H+}$, nevertheless the sub-microsecond component decay is absent in the transient of Fig. 10 while a slower component, τ_{2H+}, has appeared. The effect of protonation is mainly witnessed by a lengthening of both excited state lifetimes (from $\tau_1 = 0.24 \pm 0.06$ μs and $\tau_2 = 1.5 \pm 0.2$ μs in the absence of HClO$_4$ to $\tau_{1H+} = 1.6 \pm 0.2$ μs and $\tau_{2H+} = 15 \pm 1$ μs). Our TD-DFT calculations show that the singlet-singlet electronic transitions accounted by the MLCT(phz) state are shifted to higher energies by protonation, *i.e.* $\lambda_{calc} = 399.7$ nm for **(py)$_3$-Redppz$^+$**, $\lambda_{calc} = 396.8$ nm for **(pyH)$_2$-pyRedppz^{3+}** (effect of the protonation of free py) and $\lambda_{calc} = 297.3$

nm for **(pyH)$_2$-pyRedppzH^{4+}** (contributing only to the 17% of that electronic transition), Table 1. For **(pyH)$_2$-pyRedppzH$_2^{5+}$**, MLCT (phz) lies well below 300 nm. Conversely, ^{1}IL($\pi\pi^*$) transitions are lowered in energy after protonation (See Table 1). The net result is that ^{1}MLCT(phz) are higher in energy than ^{1}IL($\pi\pi^*$) for **(pyH)$_2$-pyRedppzH^{4+}**. The results of TD-DFT calculations contrast with the stabilization effect (*vide supra*) of MLCT(phz) by H-bonding interactions through aza N of dppz. In any case, DFT calculations suggest that protonation of aza N of dppz stabilize ^{1}IL($\pi\pi^*$) and

Fig. 12. Transient spectra recorded at different delays after the laser pulse in flash photolysis experiments of **P4VP-Re(dppz)** in deaerated DFM containing TEOA 0.075 M and HClO$_4$ 0.05 M. Insets show oscilographic traces at λ_{ob} = 450 and 600 nm in the 0–10 μs time range (left panel) and in the 0–200 μs time range (right panel). See text for details.

destabilize ^{1}MLCT(phz), thus breaking the equilibrium between ^{3}IL ($\pi\pi^*$) and ^{3}MLCT(phz) [52].

Nevertheless, in the presence of the sacrificial reductant triethanolamine (TEOA) (0.075 M in DMF), FP experiments of **P4VP-Re(dppz)** showed the formation of a transient with four absorption maxima, λ_{max} = 420, 450, 590 and 610 nm, Fig. 11. This transient spectrum experienced some transformations in the first 10 μs and the final spectrum of this transformations grew in the 10–50 μs time range and thereafter experienced a first order decay to the final product in the 50–400 μs time range. Fig. 12 shows the transient spectra in FP experiments of **P4VP-Re(dppz)** solutions in the presence of TEOA (0.075 M in DMF) and 0.05 M of HClO$_4$ in DMF. The spectra of this transient is very similar in shape to the one in Fig. 11 after the first 10 μs. However, in Fig. 12 there is nearly a ratio of 1 between the peaks at 600 nm and 430, while in Fig. 11 this ratio is nearly 2. The transient of Fig. 12 decays completely to ΔA_{inf} = 0 by a second order kinetics.

3.2.4. Pulse radiolysis experiments

The spectra of the species produced by the one-electron reduction of **-Re(CO)$_3$(dppz)$^+$** chromophores present in **P4VP-Re (dppz)** were investigated by pulse radiolysis of the polymers solutions in CH$_3$OH. Chromophores **-Re(CO)$_3$(dppz)$^+$** in polymer **P4VP-Re(dppz)** failed to react with the pulse radiolytically generated C$^•$H$_2$OH radicals. They were reduced however by e^-_{solv} at a diffusion-controlled rate. In N$_2$ deaerated methanolic solutions, the reaction between e^-_{solv} and **P4VP-Re(dppz)** was completed within the first μs after the radiolytic pulse. Due to the low solubility of **P4VP-Re(dppz)** in methanol, the concentration of Re(I) pendants was not enough to maintain a pseudo-first order kinetic in the thermal reaction with solvated electrons. The transient spectrum generated by the reaction with e^-_{solv} exhibited two absorption bands with λ_{max} = 305 and 405 nm and a shoulder at $\lambda_{max} \sim$ 550 nm. In the 5–50 μs time range the high energy band experiences little if any change, while the low energy band shifts from λ_{max} = 405 nm to λ_{max} = 415 nm, the shoulder at $\lambda_{max} \sim$ 550 nm disappears and a shoulder at $\lambda_{max} \sim$ 470 nm is evident. In addition, the solution is bleached at λ_{max} = 360 nm, Fig. 13.

3.2.5. Thermal and excited state redox reactions

PR experiments (Fig. 13) showed a transient generated by the reaction of **P4VP-Re(dppz)** with e^-_{solv} characteristic of a the reduced radical in the phz part of the dppz ligand [51]. $^•$CH$_2$OH were unable to reduce the Re(I) chromophore. Spectral changes in

the 5–50 μs time range of Fig. 13 can be accounted by H-abstraction and/or proton assisted electron transfer reactions to yield **-Re(CO)$_3$(dppzH)$^•$** and/or **-Re(CO)$_3$(dppzH)$^{•+}$** chromophores in the polymer strands of **P4VP-Re(dppz)**.

FP experiments of **P4VP-Re(dppz)**/TEOA/DMF solutions (Fig. 11) showed the formation of a transient with λ_{max} = 420, 450, 590 and 610 nm which, in the first 10 μs, experienced some spectral transformation. After 10 μs, the bands peak at λ_{max} = 440, 590 and 610 nm. It is evident that the excited state reduction by TEOA yields different species than the thermal reduction with e^-_{solv}. In fact, the transient of Fig. 11 shows spectral features of an admixture of reduced species, one species with the electron located at the phz part of dppz (λ_{max} = 440 nm) an another species with the electron located at the phen part of dppz (λ_{max} = 590 and 610 nm) since reduced radicals species of phen ligands show characteristic absorptions with $\lambda_{max} \sim$ 590–610 [53]. Therefore, it appears that both excited states, ^{3}MLCT(phz) and ^{3}MLCT(phen) are reduced by TEOA. Spectral changes of Fig. 11 can be accounted by protonation reactions of those reduced species.

A growth of the **-Re(CO)$_3$(dppz)$^•$** spectrum within the first 5–30 μs after the laser flash in flash photolysis experiments (right inset to Fig. 11) can be explained by additional reduction of **-Re(CO)$_3$(dppz)$^+$** groups by reducing TEOA$^•$ radicals generated by a reaction of TEOA$^{•+}$ with TEOA [53,54], Eqs.(2)–(3)

$$(CH_2OHCH_2)_3N^{•+} + TEOA \rightarrow (CH_2OHCH_2)_2N(^•CHOHCH_2) + TEAH^+ \quad (2)$$

$$-Re(CO)_3(dppz)^+ + (CH_2OHCH_2)_2N(^•CHOHCH_2) \rightarrow -Re(CO)_3(dppz)^• + (CH_2OHCH_2)_2N-CH=CHOH + H^+ \quad (3)$$

The demise of TEOA$^•$ radicals by disproportionation [54], Eq. (4), is in competition with the reduction process of Eq. (3)

$$(CH_2OHCH_2)_2N(^•CHOHCH_2) \rightarrow TEOA + (CH_2OHCH_2)_2N-CH=CHOH \quad (4)$$

A disproportionation reaction of -Re(CO)$_3$(dppz)$^•$ radicals [53,55,56], Eqs. (5)–(6), may occur sequentially:

$$-Re(CO)_3(dppz)^• + TEOAH^+ \rightarrow -Re(CO)_3(dppzH)^{•+} + TEOA \quad (5)$$

$$Re(CO)_3(dppzH)^{•+} \rightarrow -Re(CO)_3(dppzH_2)^+ + -Re(CO)_3(dppz)^+ \quad (6)$$

Eqs. (5)–(6) represent the protonation of -Re(CO)$_3$(dppz)$^•$ by available TEOAH$^+$ in the polymer and the slow diffusive motion of the polymeric strands that allows a bimolecular encounter of -Re(CO)$_3$(dppzH)$^{•+}$ pendants, respectively, leading to the final product of Fig. 11 in the 50–400 μs time range.

FP experiments in the system **P4VP-Re(dppz)**/TEOA/HClO$_4$/DMF (Fig. 12) are somewhat different than those of the **P4VP-Re(dppz)**/TEOA/DMF system (Fig. 11). Comparison of Fig. 11 and 12 shows that: (i) the transient of Fig. 12 is similar in spectral shape to the transient of Fig. 11 10 μs after the laser shot, though the ratio between absorbance intensities ($\Delta A_{600nm}/\Delta A_{440nm}$) is different from both figures, (ii) the transient of Fig.12 does not experience any spectral changes in the 0–10 μs time range and (iii) the transient of Fig. 12 decays by a second order kinetics law completely to ΔA = 0. The differences remarked above in (i)-(iii) can be rationalized by the following: (i) after protonation, the feasibility of MLCT(phz) reduction by TEOA is enhanced by protonation of aza N of dppz, (ii) in HClO$_4$ media, protonation of -Re(CO)$_3$(dppz)$^•$ occur rapidly (within the laser lifetime) due to the high concentration of available H$^+$ and (iii) due to the higher concentration of -Re(CO)$_3$(dppzH)$^{•+}$ pendants in FP experiments with **P4VP-Re(dppz)**/TEOA/HClO$_4$/DMF than with **P4VP-Re(dppz)**/TEOA/DMF, -Re(CO)$_3$(dppzH)$^{•+}$ chromophores are
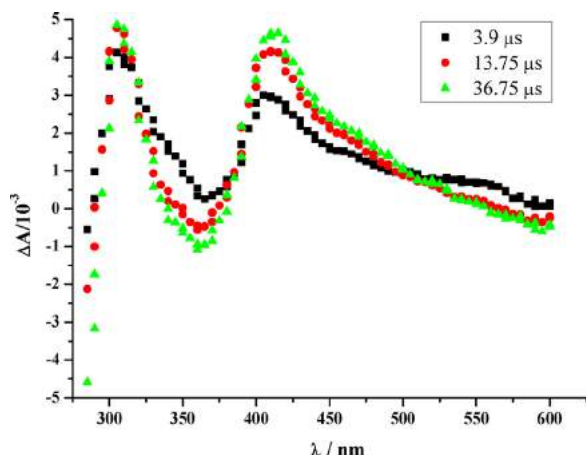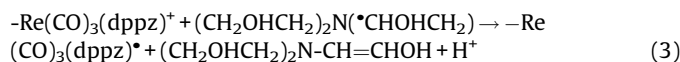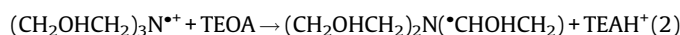

Fig. 13. Transient spectra recorded at different delays after the radiolytic pulse in pulse radiolysis experiments of N$_2$-deaerated methanolic solutions of **P4VP-Re(dppz)**. See text for details.
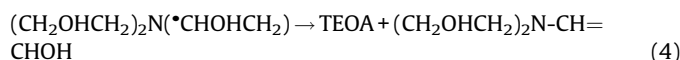
in closer proximity in the former than in the latter and a second order kinetics is favored against a disappearance by a first order decay.

4. Conclusions

A new polymer, **P4VP-Re(dppz),** based on the poly-4-vinyl-pyridine structure containing -Re(CO)$_3$(dppz)$^+$ pendants was synthesized and characterized by EA, FTIR, TEM and AFM. In DCM, AFM experiments show the formation of pearl-necklace rings. Multiple morphologies of **P4VP-Re(dppz),** such as vesicles, spherical nanoaggregates, large vesicle compounds, rings and pyramidal structures were observed by AFM and TEM in cast films of **P4VP-Re(dppz)** in solvents of different polarity and solvent/acid mixtures. In neat DMF, vesicles of low polydispersity were clearly observed from aggregation of **P4VP-Re(dppz)** strands by TEM experiments. This is a distinctive and very interesting feature of **P4VP-Re(dppz)** as compared to our previously studied Re(I) polymers which tend to form highly poly-disperse aggregates. Protonation of DMF **P4VP-Re(dppz)** solutions show a shrinkage of those vesicles to form smaller spherical nanodomains which are coexisting with LCV. Those morphological changes were mimicked by DFT calculations on several fractions of the Re(I) polymers under different degrees of protonation. An expansion of the poly-4-vinylpyridine backbone is predicted after protonation by DFT calculations in agreement with TEM observations. FP experiments were also dependent on the protonation state of the polymer. In neat DMF a transient of ^{3}IL character decayed with lifetimes of $\tau_1 = 0.24\,\mu s$ and $\tau_2 = 1.5\,\mu s$ while in DMF/HClO$_4$ solutions the lifetimes were 1.6 and 15 μs, respectively. The reductive quenching of the excited states of **P4VP-Re(dppz)** was studied in FP experiments in the presence of TEOA either in DMF or DMF/HClO$_4$ solutions. FP experiments with TEOA in neat DMF were contrasted to PR experiments in MeOH. While PR experiments show a transient characteristic of a species where the reduction occurred in the phz part of dppz, FP experiments in TEOA/DMF system show a transient which can be ascribed to an admixture of reduced species, one species with the electron located at the phz part of dppz and another species with the electron located at the phen part of dppz. Therefore, it appears that both excited states, ^{3}MLCT (phz) and ^{3}MLCT(phen) are reduced by TEOA. In FP experiments of **P4VP-Re(dppz)** with TEOA/DMF/HClO$_4$ solutions the feasibility of MLCT(phz) reduction by TEOA is enhanced by protonation of aza N of dppz.

Acknowledgements

Appendix A. Supplementary data

Supplementary data associated with this article can be found, in the online version, at https://doi.org/10.1016/j.jphoto-chem.2017.11.007.

References

[1] A.W. McKinley, P. Lincoln, E.M. Tuite, Environmental effects on the photophysics of transition metal complexes with dipyrido[2,3-a:3′,2′-c] phenazine (dppz) and related ligands, Coord. Chem. Rev. 255 (2011) 2676–2692.

[2] V. Wing-Wah Yam, K. Kam-Wing Lo, K.-K. Cheung, R. Yuen-Chong Kong, Deoxyribonucleic acid binding and photocleavage studies of rhenium(I) dipyridophenazine complexes, J. Chem. Soc. Dalton Trans. (1997) 2067–2072.

[3] G.T. Ruiz, M.P. Juliarena, R.O. Lezna, E. Wolcan, M.R. Feliz, G. Ferraudi, Intercalation of fac-[(4,4′-bpy)Re^I(CO)$_3$(dppz)]$^+$, dppz = dipyridyl[3,2-a:2′3′-c] phenazine, in polynucleotides on the UV–vis photophysics of the Re(I) intercalator and the redox reactions with pulse radiolysis-generated radicals, Dalton Trans. (2007) 2020–2029.

[4] C. Metcalfe, M. Webb, J.A. Thomas, A facile synthetic route to bimetallic Re^I complexes containing two dppz DNA intercalating ligands, Chem. Commun. (2002) 2026–2027.

[5] J.A. Smith, M.W. George, J.M. Kelly, Transient spectroscopy of dipyridophenazine metal complexes which undergo photo-induced electron transfer with DNA, Coord. Chem. Rev. 255 (2011) 2666–2675.

[6] H.D. Stoeffler, N.B. Thornton, S.L. Temkin, K.S. Schanze, Unusual photophysics of a Rhenium(I) dipyridophenazine complex in homogeneous solution and bound to DNA, J. Am. Chem. Soc. 117 (1995) 7119–7128.

[7] H. van der Salm, M.G. Fraser, R. Horvath, S.A. Cameron, J.E. Barnsley, X.-Z. Sun, M.W. George, K.C. Gordon, Re(I) complexes of substituted dppz: a computational and spectroscopic study, Inorg. Chem. 53 (2014) 3126–3140.

[8] G.T. Ruiz, G. Ferraudi, E. Wolcan, M.R. Féliz, On the elusive non-emissive yet reactive, upper excited states of (4,4′-bpy)Re^I(CO)$_3$(dppz) PF$_6$ (dppz = dipyridil 3,2-a:2′3′-c phenazine), Inorg. Chim. Acta 363 (2010) 1615–1618.

[9] C. Hiort, P. Lincoln, B. Norden, DNA binding of Δ- and Λ- [Ru(phen)$_2$DPPZ]$^{2+}$, J. Am. Chem. Soc. 115 (1993) 3448–3454.

[10] J. Dickeson, L. Summers, Derivatives of 1,10-phenanthroline-5,6-quinone, Aust. J. Chem. 23 (1970) 1023–1027.

[11] M.P. McCurdie, L.A. Belfiore, Spectroscopic analysis of transition-metal coordination complexes based on poly(4-vinylpyridine) and dichlorotricarbonylruthenium(II), Polymer 40 (1999) 2889–2902.

[12] G.V. Buxton, C.L. Greenstock, W.P. Helman, A.B. Ross, Critical Review of rate constants for reactions of hydrated electrons, hydrogen atoms and hydroxyl radicals (●OH/●O−) in Aqueous Solution, J. Phys. Chem. Ref. Data 17 (1988) 513–886.

[13] G.L. Hug, Y. Wang, C. Schöneich, P.-Y. Jiang, R.W. Fessenden, Multiple time scales in pulse radiolysis. Application to bromide solutions and dipeptides, Radiat. Phys. Chem. 54 (1999) 559–566.

[14] M.R. Féliz, G. Ferraudi, Charge-Transfer Processes in (4-Nitrobenzoate)Re (CO)$_3$(azine)$_2$Complexes. Competitive Reductions of 4-Nitrobenzoate and Azine in Thermally and Photochemically Induced Redox Processes, Inorg. Chem. 37 (1998) 2806–2810.

[15] N. Getoff, A. Ritter, F. Schwörer, P. Bayer, Primary yields of CH$_3$●O and ●CH$_2$OH radicals resulting in the radiolysis of high purity methanol, Radiat. Phys. Chem. 41 (1993) 797–801.

[16] L.M. Dorfman, The solvated electron in organic liquids, in: R.F. Gould (Ed.), Advances in Chemistry Series 50, American Chemical Society, Washington, DC, 1965, pp. 36–44.

[17] M. Simic, P. Neta, E. Hayon, Pulse radiolysis study of alcohols in aqueous solution, J. Phys. Chem. 73 (1969) 3794–3800.

[18] Y. Gao, S. Sun, K. Han, Electronic structures and spectroscopic properties of rhenium (I) tricarbonyl photosensitizer: [Re(4,4′-(COOEt)−2,2′-bpy)(CO)$_3$py] PF$_6$, Spectrochim. Acta A 71 (2009) 2016–2022.

[19] A. Vlcek Jr., S. Zális, Modeling of charge-transfer transitions and excited states in d^6 transition metal complexes by DFT techniques, Coord. Chem. Rev. 251 (2007) 258–287.

[20] J. Dietrich, U. Thorenz, C. Förster, K. Heinze, Effects of sequence, connectivity, and counter ions in new amide-Linked Ru(tpy)$_2$–Re(bpy) chromophores on redox chemistry and photophysics, Inorg. Chem. 52 (2013) 1248–1264.

[21] D. Chartrand, C.A. Castro Ruiz, G.S. Hanan, Diimine triscarbonyl Re(I) of isomeric pyridyl-fulvene ligands: an electrochemical, spectroscopic, and computational investigation, Inorg. Chem. 51 (2012) 12738–12747.

[22] C. Zhao, C.S. Kambara, Y. Yang, A.L. Kaledin, D.G. Musaev, T. Lian, C.L. Hill, Synthesis, structures, and photochemistry of tricarbonyl metal polyoxoanion complexes, [X$_2$W$_{20}$O$_{70}${M(CO)$_3$}$_2$]$^{12-}$(X = Sb, Bi and M = Re, Mn), Inorg. Chem. 52 (2013) 671–678.

[23] C.B. Anderson, A.B.S. Elliott, C.J. McAdam, K.C. Gordon, J.D. Crowley, Fac-Re(CO) 3Cl complexes of [2-(4-R-1H-1,2,3-triazol-1-yl)methyl]pyridine inverse click ligands: a systematic synthetic, spectroscopic, and computational study, Organometallics 32 (2013) 788–797.

[24] L. Yang, A.–M. Ren, J.–K. Feng, X.–D. Liu, Y.–G. Ma, H.-X. Zhang, Theoretical studies of ground and excited electronic states in a series of Rhenium(I) bipyridine complexes containing diarylethynyl-based structure, Inorg. Chem. 43 (2004) 5961–5972.

[25] L. Yang, A.-M. Ren, J.-K. Feng, X.-J. Liu, Y.-G. Ma, M. Zhang, X.-D. Liu, J.-C. Shen, H.-X. Zhang, Theoretical studies of ground and excited electronic states in a series of halide Rhenium(I) bipyridine complexes, J. Phys. Chem. A 108 (2004) 6797–6808.

[26] S. Záliš, C.J. Milne, A. El Nahhas, A.M. Blanco-Rodríguez, R.M. van der Veen, A. Vlček, Re and Br X-ray absorption near-edge structure study of the ground and

excited states of [ReBr(CO)$_3$(bpy)] interpreted by DFT and TD-DFT calculations, Inorg. Chem. 52 (2013) 5775–5785.

[27] J. Bossert, C. Daniel, Trans-cis photoisomerization of the styrylpyridine ligand in [Re(CO)$_3$(2,2′-bipyridine)(t-4-styrylpyridine)]$^+$: role of the metal-to-ligand charge-transfer excited states, Chem. Eur. J. 12 (2006) 4835–4843.

[28] P. Hohenberg, W. Kohn, Inhomogeneous electron gas, Phys. Rev. 136 (1964) B864–B871.

[29] W. Kohn, L.J. Sham, Self-consistent equations including exchange and correlation effects, Phys. Rev. 140 (1965) A1133–A1138.

[30] R.G. Parr, W. Yang, Density Functional Theory of Atoms and Molecules, Oxford University Press, 1989.

[31] M.J. Frisch, G.W. Trucks, H.B. Schlegel, G.E. Scuseria, M.A. Robb, J.R. Cheeseman, G. Scalmani, V. Barone, B. Mennucci, G.A. Petersson, H. Nakatsuji, M. Caricato, X. Li, H.P. Hratchian, A.F. Izmaylov, J. Bloino, G. Zheng, J.L. Sonnenberg, M. Hada, M. Ehara, K. Toyota, R. Fukuda, J. Hasegawa, M. Ishida, T. Nakajima, Y. Honda, O. Kitao, H. Nakai, T. Vreven, J.J.A. Montgomery, J.E. Peralta, F. Ogliaro, M. Bearpark, J.J. Heyd, E. Brothers, K.N. Kudin, V.N. Staroverov, T. Keith, R. Kobayashi, J. Normand, K. Raghavachari, A. Rendell, J.C. Burant, S.S. Iyengar, J. Tomasi, M. Cossi, N. Rega, J.M. Millam, M. Klene, J.E. Knox, J.B. Cross, V. Bakken, C. Adamo, J. Jaramillo, R. Gomperts, R.E. Stratmann, O. Yazyev, A.J. Austin, R. Cammi, C. Pomelli, J.W. Ochterski, R.L. Martin, K. Morokuma, V.G. Zakrzewski, G.A. Voth, P. Salvador, J.J. Dannenberg, S. Dapprich, A.D. Daniels, O. Farkas, J.B. Foresman, J.V. Ortiz, J. Cioslowski, D.J. Fox, Gaussian 09, Revision A1, Gaussian, Inc., Wallingford CT, 2009.

[32] A.D. Becke, Density-functional thermochemistry. III. The role of exact exchange, J. Chem. Phys. 98 (1993) 5648–5652.

[33] C. Lee, W. Yang, R.G. Parr, Development of the Colle-Salvetti correlation-energy formula into a functional of the electron density, Phys. Rev. B 37 (1988) 785–789.

[34] T.H. Dunning Jr, P.J. Hay, in: H.F. Schaefer III (Ed.), Methods of Electronic Structure Theory, Plenum Press, 1977.

[35] P.J. Hay, W.R. Wadt, Ab initio effective core potentials for molecular calculations. Potentials for the transition metal atoms Sc to Hg, J. Chem. Phys. 82 (1985) 270–283.

[36] P.J. Hay, W.R. Wadt, Ab initio effective core potentials for molecular calculations. Potentials for K to Au including the outermost core orbitals, J. Chem. Phys. 82 (1985) 299–310.

[37] W.R. Wadt, P.J. Hay, Ab initio effective core potentials for molecular calculations. Potentials for main group elements Na to Bi, J. Chem. Phys. 82 (1985) 284–298.

[38] R. Bauernschmitt, R. Ahlrichs, Treatment of electronic excitations within the adiabatic approximation of time dependent density functional theory, Chem. Phys. Lett. 256 (1996) 454–464.

[39] M.E. Casida, C. Jamorski, K.C. Casida, D.R. Salahub, Molecular excitation energies to high-lying bound states from time-dependent density-functional response theory: characterization and correction of the time-dependent local density approximation ionization threshold, J. Chem. Phys. 108 (1998) 4439–4449.

[40] R.E. Stratmann, G.E. Scuseria, M.J. Frisch, An efficient implementation of time-dependent density-functional theory for the calculation of excitation energies of large molecules, J. Chem. Phys. 109 (1998) 8218–8224.

[41] V. Barone, M. Cossi, Quantum calculation of molecular energies and energy gradients in solution by a conductor solvent model, J. Phys. Chem. A 102 (1998) 1995–2001.

[42] M. Cossi, V. Barone, Time-dependent density functional theory for molecules in liquid solutions, J. Chem. Phys. 115 (2001) 4708–4717.

[43] B. Mennucci, J. Tomasi, Continuum solvation models: a new approach to the problem of solute's charge distribution and cavity boundaries, J. Chem. Phys. 106 (1997) 5151–5158.

[44] E. Wolcan, M.R. Feliz, J.L. Alessandrini, G. Ferraudi, Aggregation in nanobundles and the effect of diverse environments on the solution-phase photochemistry and photophysics of −Re(CO)$_3$L$^+$(L = 1,10-phenanthroline, 2,2′-bipyridine) pendants bonded to poly(4-vinylpyridine), Inorg. Chem. 45 (2006) 6666–6677.

[45] E. Wolcan, J.L. Alessandrini, M.R. Féliz, On the quenching of MLCT$_{Re-bpy}$ luminescence by Cu(II) species in Re(I) polymer micelles, J. Phys. Chem. B 109 (2005) 22890–22898.

[46] L.L.B. Bracco, M.P. Juliarena, G.T. Ruiz, M.R. Féliz, G.J. Ferraudi, E. Wolcan, Resonance energy transfer in the solution phase photophysics of −Re(CO)$_3$L$^+$ pendants bonded to poly(4-vinylpyridine), J. Phys. Chem. B 112 (2008) 11506–11516.

[47] A. Vlček, Ultrafast excited-State processes in Re(I) carbonyl-diimine complexes: from excitation to photochemistry, in: A.J. Lees (Ed.), Photophysics of Organometallics, Springer, Berlin/Heidelberg, 2010, pp. 73–114.

[48] A. Kumar, S.-S. Sun, A. Lees, Photophysics and photochemistry of organometallic rhenium diimine complexes, in: A.J. Lees (Ed.), Photophysics of Organometallics, Springer, Berlin/Heidelberg, 2010, pp. 37–71.

[49] H.H. Martinez Saavedra, C.A. Franca, G. Petroselli, R. Erra-Balsells, G.T. Ruiz, E. Wolcan, A new zwitterionic, water soluble, Re(I) complex: synthesis, spectroscopic and computational characterization, J. Organomet. Chem. 745–746 (2013) 470–478.

[50] E. Wolcan, On the origins of the absorption spectroscopy of pterin and Re(CO)3 (pterin)(H2O) aqueous solutions. A combined theoretical and experimental study, Spectrochim. Acta A 129 (2014) 173–183.

[51] M.P. Juliarena, R.O. Lezna, M.R. Feliz, G.T. Ruiz, S. Thomas, G. Ferraudi, I. Carmichael, On the association and structure of radicals derived from dipyridil [3,2-a:2′3′-c]phenazine. Contrast between the electrochemical, radiolytic, and photochemical reduction processes, J. Org. Chem. 71 (2006) 2870–2873.

[52] J. Dyer, W.J. Blau, C.G. Coates, C.M. Creely, J.D. Gavey, M.W. George, D.C. Grills, S. Hudson, J.M. Kelly, P. Matousek, J.J. McGarvey, J. McMaster, A.W. Parker, M. Towrie, J.A. Weinstein, The photophysics of fac-[Re(CO)3(dppz)(py)]$^+$ in CH$_3$CN: a comparative picosecond flash photolysis, transient infrared, transient resonance Raman and density functional theoretical study, Photochem. Photobiol. Sci. 2 (2003) 542–554.

[53] E. Wolcan, G. Ferraudi, Photochemical and photophysical properties of Fac-Re (I) tricarbonyl complexes: a comparison of monomer and polymer species with − ReI(CO)3phen chromophores, J. Phys. Chem. A 104 (2000) 9285–9286.

[54] L.L.B. Bracco, M.R. Féliz, E. Wolcan, On the quenching of MLCT luminescence by amines: the effect of nanoaggregation in the decrease of the reorganization energy, J. Photochem. Photobiol. A 210 (2010) 23–30.

[55] J. Guerrero, O.E. Piro, E. Wolcan, M.R. Feliz, G. Ferraudi, S.A. Moya, Photochemical and photophysical reactions of fac-rhenium(I) tricarbonyl complexes. Effects from binucleating spectator ligands on excited and ground state processes, Organometallics 20 (2001) 2842–2853.

[56] M. Feliz, G. Ferraudi, H. Altmiller, Primary photochemical processes in fac-ClRe (CO)$_3$L$_2$ (L = 4-phenylpyridine and 4-cyanopyridine): a steady-state and flash photochemical study of reaction products and intermediates, J. Phys. Chem. 96 (1992) 257–264.